ELSEVIER

Chemical Geology 177 (2001) 351–370

CHEMICAL GEOLOGY
INCLUDING
ISOTOPE GEOSCIENCE

www.elsevier.com/locate/chemgeo

Halogen and Ar–Ar age determinations of inclusions within quartz veins from porphyry copper deposits using complementary noble gas extraction techniques

M.A. Kendrick *, R. Burgess, R.A.D. Pattrick, G. Turner

Department of Earth Sciences, University of Manchester, Oxford Road, Manchester, M13 9PL, UK

Accepted 1 November 2000

Abstract

Extension of Ar–Ar methodology has been used to determine mineralisation ages from mica inclusions and to simultaneously evaluate the noble gas and halogen composition of inclusion fluids within irradiated quartz vein samples from five porphyry copper deposits. Samples have been collected from the potassic and propylitic zones of Bingham Canyon, Utah, and four Arizonan deposits; Silverbell, Globe-Miami, Pinto Valley and Ray. Data obtained using three noble gas extraction techniques (laser ablation, in vacuo crushing and stepped heating) are compared with each other. Laser ablation provides a means for the analysis of individual fluid inclusions but is limited by blank levels and detection limits. Stepped heating and in vacuo crushing are bulk extraction techniques that preferentially release gases from solid and fluid inclusion phases, respectively, and can be used in combination to obtain accurate and meaningful ages of mineralisation. Ages obtained for porphyry copper deposits are as follows: Bingham Canyon 37.1 ± 0.5, Ray 65.3 ± 1.5, Globe-Miami 61.7 ± 3.4, Pinto Valley 63.2 ± 8.0 and Silverbell 55.8 ± 1.8. The age of mineralisation at Ray is of particular interest as it enables a reported discrepancy in K–Ar ages to be understood. Halogen data for the Bingham Canyon samples gives insight into the partitioning of the heavy halogens (Br and I) between solid and liquid phases.

Keywords: Ar–Ar; Fluid inclusions; Quartz; Halogens; Porphyry; Noble gases

1. Introduction

The conservative behaviour of noble gases has made them useful in the study of modern and ancient groundwaters (Andrews and Lee, 1979; Kennedy et al., 1985; Mazor, 1972; Mazor and Wasserburg, 1965; O'Nions and Ballentine, 1993; Zaikowski et al., 1987). Likewise, halogens exhibit conservative behaviour, albeit to a lesser degree than the noble gases, and are well established geochemical tracers used in studies of both modern ground water and ancient mineralising systems (Crocetti and Holland, 1989; Fontes and Matray, 1993; Kesler et al., 1995; Viets et al., 1996). Together, the noble gases and halogens can provide information on the age of mineralisation, the fluid's source and the acquisition of salinity.

* Corresponding author.

0009-2541/01/$ - see front matter
PII: S0009-2541(00)00419-8

Irradiation of samples with neutrons prior to analysis enables simultaneous determination of both the naturally occurring noble gas isotopes (^{40}Ar, ^{36}Ar, ^{84}Kr, ^{129}Xe), the halogens (Cl, Br, I) and other cations (K, U) by noble gas mass spectrometry (Bohlke and Irwin, 1992a,b; Kelley et al., 1986; Turner and Bannon, 1992). The high sensitivity of this technique, which is an extension of Ar–Ar methodology, makes it ideal for studying the small sample sizes available in fluid inclusions. Quartz is potentially a good mineral for these studies because it has a high abundance of fluid inclusions and the lattice tends to be relatively free from impurities. Neutron induced and natural noble gas isotopes released during analysis will therefore have originated in the fluid inclusions and not the lattice; the sample also has low radioactivity after irradiation.

A method for dating vein quartz is highly desirable because quartz is a common gangue mineral in many hydrothermal deposits and determining the age of mineralisation is often difficult using conventional isotopic dating techniques. Qui (1996) proposed an Ar–Ar method of dating quartz based on in vacuo crushing. However, in many cases, the presence of excess ^{40}Ar ($^{40}Ar_E$), which is not attributable to in situ radioactive decay of ^{40}K or atmospheric contamination, precludes an accurate age determination (Rama et al., 1965), particularly during crushing experiments.

In vacuo crushing and stepped heating are bulk extraction techniques that provide compositional information for selected inclusion fluids and solid phases, which to a degree can be deconvolved by the use of isotope mixing diagrams. When used in combination, the bulk extraction techniques are especially useful as a means of extracting age information in the presence of $^{40}Ar_E$ (Kelley et al., 1986; Turner, 1988; Turner and Bannon, 1992). Laser ablation enables individual or groups of related fluid inclusions to be targeted, but it is a technically demanding procedure and a relatively large number of analyses must be undertaken to obtain average compositions for the different fluid inclusion populations (Bohlke and Irwin, 1992a).

The complimentary nature of the three extraction techniques has been investigated in detail to give a better understanding of the efficiency with which laser, stepped heating and in vacuo crushing release noble gases from fluid and solid phases. We also show how noble gas extraction techniques can be combined to obtain maximum information on both chronology and fluid history. The laser extraction technique has been applied to a quartz vein from the potassic alteration zone of the Bingham Canyon porphyry copper deposit in Utah with the objective of determining variations in noble gas and halogen composition of the fluids across the vein. Successful age determinations have been obtained from Bingham Canyon and for four other porphyry copper deposits from Arizona for which samples were available from both the potassic and propylitic alteration zones. The geological significance of the fluid inclusion noble gas and halogen compositions of these and other samples will provide the focus for a subsequent paper (Kendrick et al., 2001).

2. Samples

Quartz vein samples have been collected from the potassic and propylitic alteration zones of five porphyry copper deposits; Bingham Canyon (BC) in Utah, and Silverbell (SB), Globe-Miami (GM), Pinto Valley (PV) and Ray (R), in Arizona. Prior to noble gas analysis, characterisation of fluid inclusion populations and limited thermometric determinations enabled average salinities to be estimated (Table 1).

Samples were crushed, and quartz chips (1–3 mm size, total 60–90 mg) were selected for purity under a binocular microscope. Following irradiation, vein chips were analysed by two bulk extraction techniques, in the order of in vacuo crushing and then stepped heating. Additionally, a single 5-cm wide quartz vein (sample BC5) from the potassic alteration zone of Bingham Canyon, was cut into three wafers (300 μm) and studied in detail using a combination of three extraction techniques, in the order: laser microprobe, in vacuo crushing, and stepped heating. Samples BC5-A and BC5-C are from the margins of the vein while sample BC5-B is from the centre of the vein.

Although sample thin sections appeared free from contaminating minerals, the high K contents and the high K/Cl ratios (>1) measured during step heating (Table 1), indicate that in addition to sylvite identified in fluid inclusions, a second K rich, Cl poor

Table 1
Sample characteristics

Sample	Vein	Fluid inclusion frequency			Average salinity (wt.% NaCl equiv.)[a]	K content (step heating)[b]	
		LV	V	LVD		wt.% K	K/Cl
BC5-A, BC5-B, BC5-C	5-cm wide molybdenite bearing quartz vein. Central potassic zone	high	high	high	17	0.01	0.29
BC4	Quartz vein (~ 1 cm) hosted by highly altered monzonite; potassic zone, with a late sericitic overprint.	high	high	low	14	0.08	8
BC3	Chalcopyrite and molybdenite bearing quartz veinlets hosted by potassically altered monzonite.	high	high	high	14	0.73	95
BC2	Quartz veinlet through equigranular monzonite of the propylitic zone. Associated with pyrite stringers, 0.1% Cu.	Dom.	rare	zero	2	4.27	720
R1	Pyrite bearing quartz vein hosted by potasically altered granite mountian porphyry.	Dom.	rare	rare	10	0.56	102
R3	Pyrite bearing quartz vein hosted by propolytically altered pinal schist.	Dom.	none	none	5	0.35	212
GM3	Chalcopyrite and pyrite bearing quartz vein. Potassic zone, Blue bird live oak pit.	high	Mod.	low	10	0.04	30
GM4	Pyrite bearing quartz vein, taken from the propylitic zone. Intermediate with the potassic zone.	Dom.	none	rare	6	0.94	267
PV6	Chalcopyrite bearing quartz vein from ore zone. Hosted by potassically altered quartz monzonite.	Dom.	low	low	12	0.03	71
PV1	Pyrite bearing quartz vein, phyllic vein selvage. Hosted by precambrian Gulch granite.	Dom.	low	rare	5	0.02	47
SB4	Pyrite bearing quartz vein hosted by potassically altered alaskite.	Dom.	none	none	11	0.07	14
SB1	Pyrite and chalcocite bearing quartz vein from central monzonite, potassic zone.	–	–	–	–	0.41	141
SB8	Quartz vein from dacite in outer propylitic zone.	–	–	–	–	0.75	216
SB6	Quartz vein from outside edge of monzonite, propylitic zone.	High (2°)	none	none	5?	0.004	0.83

[a]The average salinity of fluid inclusions expressed as wt.% NaCl equiv. based on a thermometric study and the relative abundance of three fluid inclusion types: LV—liquid vapour, V—vapour dominated and LVD—liquid vapour and a daughter mineral.
[b]The wt.% K is a fraction of the solid phase, i.e. quartz matrix plus solid inclusions.

phase is present. It is believed this phase (mica or K-feldspar) is present as micron-sized inclusions within the quartz, in the more potassic samples mica may also be present along grain boundaries. Assuming the solid inclusions and vein quartz are syngenetic, chronological data is made available by separating Ar from the fluid inclusions and solid phases. If all the K released by step heating is from white mica, it can be estimated that, with the exception of BC2, mica accounts for between 0.1% and 9% of the total 'quartz' vein material; approximately 10 times the wt.% K content (Table 1). The figure is lower ($< 6\%$) if K-feldspar accounts for the solid phase. On the basis of measured K, sample BC2 contains a large component of either mica or K-feldspar.

2.1. Requirements for laser ablation

Laser ablation provides a means for selectively analysing small groups of fluid inclusions, the minimum *number* of inclusions that can be analysed depends upon the spatial resolution of the laser which in the present system is about 20 μm. The

Table 2
Minimum size of measurable fluid inclusions

	Detection limit, noble gas (cm^{-3} STP)	Detection limit (parent) (g)	Concentration in seawater	Minimum diameter (μm)
$^{39}Ar(K)$	0.85×10^{-12}	9.2×10^{-6}	0.39×10^{-3} g/cc	3557
$^{38}Ar(Cl)$	0.91×10^{-13}	0.44×10^{-9}	19×10^{-3} g/cc	35
$^{80}Kr(Br)$	43×10^{-15}	2.0×10^{-12}	65×10^{-6} g/cc	39
$^{128}Xe(I)$	16×10^{-15}	2.0×10^{-12}	0.55×10^{-6} g/cc	414
^{40}Ar	0.28×10^{-9}	–	0.34×10^{-3} cc/cc	117
^{36}Ar	3.0×10^{-12}	–	1.1×10^{-6} cc/cc	171

Note: Detection limits based on $10 \times$ blank level.

minimum fluid inclusion *size* that can be analysed depends upon the salinity, neutron fluence and detection limits of the mass spectrometer. The estimates of minimum fluid inclusion size given in Table 2 depend upon the detection limits for each element or isotope, and assumes a typical fluence of 10^{18} n/cm^2 and a fluid composition of seawater. Porphyry copper ore fluids are significantly more saline than seawater and the K and I abundance is several orders of magnitude above the seawater value. Therefore, the minimum required inclusion sizes given in Table 2 should be considered as conservative upper limits.

Fluid inclusions in sample BC5 have an average salinity of 17 wt.% NaCl equiv. and it is expected that $^{38}Ar_{Cl}$ should be detectable in fluid inclusions a factor of two smaller than those calculated for the seawater concentration. Detection limits could be improved further by a factor of two or three with acceptable increases in the neutron fluence of irradiation.

3. Experimental methods

3.1. Irradiation

The samples were irradiated in position L67 of the Ford reactor, University of Michigan (irradiation designated MN11), and received a total neutron fluence of approximately 10^{18} n/cm^2. Hb3gr monitors were used to determine the irradiation parameters $J = 0.01785 \pm 0.00025$: $\beta = 4.28 \pm 0.01$ (Kelley et al., 1986). Subsequently, β and J were used to calculate the fluence of thermal neutrons, and thus to determine the abundance of Cl, Br, I and K measured as $^{38}Ar_{Cl}$, $^{80}Kr_{Br}$, $^{128}Xe_{I}$ and $^{39}Ar_{K}$, respectively. Calculated amounts of I and Br were corrected for production from resonant neutrons based on data from the Shallowater meteorite I–Xe standard. The resonant neutron flux was calculated as 2.8% of the total and correction factors of 0.56 and 0.75 were calculated for I and Br, respectively. The methods are described in detail by Johnson et al. (2000).

3.2. Noble gas extraction

Laser analysis of the Bingham Canyon samples was carried out using a Q switched Nd-YAG laser microprobe frequency quadrupled to give an output wavelength of 266 nm (UV). The focussed laser beam was targeted using a videozoom camera (Leica monozoom 7) operating in transmitted light. Laser analysis of 300-μm wafer samples was undertaken with a 10-Hz pulse rate and a pulse energy of 2 mJ over a period of 30 s. Scanning electron microscopy (SEM) photomicrographs of wafer samples revealed that laser pits of 20 μm-diameter could be drilled to a depth of 30 μm in less than 20 s. In each sample, small groups of inclusions were targeted because individual fluid inclusions yield insufficient noble gases for isotopic analysis. The extracted gas was purified on a Zr–Al getter (SAES NP10) at 400°C for 5 min before being admitted directly into the mass spectrometer.

Crushing was carried out in modified stainless steel Nupro® valves. The crushers were baked overnight at 250°C until the vacuum was $< 10^{-9}$ Torr. Noble gases were extracted by sequential crushing of the quartz samples in five steps. The

Table 3
Typical blank levels measured for the three extraction techniques

Isotope	In vacuo crushing (cm^{-3} STP)	Furnace 200°C step (cm^{-3} STP)	Furnace 1400°C step (cm^{-3} STP)	Laser (cm^{-3} STP)
^{40}Ar	0.15×10^{-9}	0.21×10^{-9}	2.3×10^{-9}	28×10^{-12}
$^{39}Ar(K)$	0.36×10^{-12}	0.58×10^{-12}	1.1×10^{-12}	85×10^{-15}
$^{38}Ar(Cl)$	0.36×10^{-12}	0.13×10^{-12}	1.2×10^{-12}	91×10^{-15}
^{36}Ar	0.37×10^{-12}	1.8×10^{-12}	9.5×10^{-12}	0.29×10^{-12}
^{84}Kr	9.2×10^{-15}	15×10^{-15}	21×10^{-15}	24×10^{-15}
$^{80}Kr(Br)$	9.2×10^{-15}	30×10^{-15}	44×10^{-15}	4.3×10^{-15}
$^{128}Xe(I)$	39×10^{-15}	39×10^{-15}	48×10^{-15}	1.6×10^{-15}

evolved gas was purified on a Zr–Al getter (SAES NP10) at 400°C for 5 min and transferred using a charcoal finger at liquid nitrogen temperature into the mass spectrometer inlet system. The gas underwent a further 5 min of purification on a second Zr getter (SAES ST172) at 250°C, before admission to the mass spectrometer.

A portion (30–50 mg) of the powdered residue from the in vacuo crushing was packed in Al foil and step-heated in a tantalum resistance furnace. Each step was of 30-min duration using a temperature range between 200°C and 1600°C at intervals of 200°C. The evolved gases were gettered (SAES NP10) at 400°C throughout the heating step and transferred over a period of 15 min to the mass spectrometer inlet using the procedure described previously for the crushing analysis.

3.3. Mass spectrometry

Isotopic analysis of Ar, Kr and Xe was performed on a single focusing, magnetic sector spectrometer (MS1). The MS1 consists of a Bauer–Signer source, a 90° sector, 15-cm radius flight tube and two detectors; a Faraday cup and a EPT AEM 1000 discrete dynode electron multiplier operating in analogue mode. During bulk analyses, Ar isotopes are measured on the Faraday cup, while the lower abundance of Kr and Xe necessitates measurement on the electron multiplier. The much lower level of gas evolved by laser extraction requires measurement of all isotopes on the electron multiplier.

Ar, Kr and Xe calibrations were undertaken at the start of every day using air aliquots. The calibration determined the sensitivity of the mass spectrometer and the mass discrimination for the Ar isotopes.

Typical blank levels for the different extraction techniques are given in Table 3. All blanks had an isotopic composition similar to that of atmosphere. Blank levels are typically $< 10\%$ of the noble gases released by crushing or stepped heating. Since the effect of a blank correction is to increase the error and shift points slightly (within error) towards a more atmospheric composition, no blank correction has been applied to the data. Blanks were measured after baking, at the start and finish of every sample analysis, and at regular intervals in between. The low abundance of noble gases liberated by laser analysis means that the level of blank is critical and it was not possible to determine accurate measurements of ^{40}Ar in fluid inclusions due to the relatively high ^{40}Ar blank.

4. Bingham Canyon halogen determinations

4.1. Laser microprobe

The extensive data are presented in Tables 4 and 5. Laser analyses of fluid inclusions give variable Br/Cl values in the range 0.50×10^{-3}–1.51×10^{-3} molar (M), with a mean of 1.1×10^{-3} M, lower than the seawater ratio of 1.54×10^{-3} M (Fig. 1). Irwin and Roedder (1995) also examined fluid inclusions in three samples of potassic zone vein quartz from Bingham using a laser technique. The first two samples had a range of Br/Cl values between 1.01 $\times 10^{-3}$ and 1.97×10^{-3} M, with mean values of

Table 4
Bingham Canyon, laser data

Sample	Cl moles ($\times 10^{-12}$)	Br moles ($\times 10^{-15}$)	K moles ($\times 10^{-12}$)	Br/Cl ($\times 10^{-3}$)	K/Cl
BC5-A					
1	347.07 ± 13.55	–	120.66 ± 12.66	–	0.35 ± 0.04
2	96.72 ± 5.45	127.68 ± 7.22	33.42 ± 1.67	1.32 ± 0.11	0.35 ± 0.03
3	570.13 ± 22.15	742.78 ± 12.61	213.58 ± 13.53	1.30 ± 0.06	0.37 ± 0.03
4	57.02 ± 2.92	56.28 ± 3.56	24.04 ± 8.72	0.99 ± 0.08	0.42 ± 0.15
5	8.21 ± 1.64	–	–	–	–
6	29.72 ± 1.91	–	25.94 ± 13.62	–	0.87 ± 0.46
7	–	28.77 ± 2.41	10.93 ± 3.53	–	–
8	172.11 ± 7.47	207.72 ± 4.25	65.19 ± 8.65	1.21 ± 0.06	0.38 ± 0.05
9	24.36 ± 1.46	26.31 ± 4.32	7.45 ± 6.31	1.08 ± 0.19	0.31 ± 0.26
10	51.89 ± 2.82	48.98 ± 3.91	21.34 ± 10.8	0.94 ± 0.09	0.41 ± 0.20
11	167.51 ± 7.41	170.89 ± 2.40	61.81 ± 7.75	1.02 ± 0.05	0.37 ± 0.04
12	23.15 ± 1.62	19.09 ± 3.56	8.53 ± 3.29	0.82 ± 0.16	0.37 ± 0.14
13	4.07 ± 0.54	6.14 ± 2.75	–	1.51 ± 0.70	–
14	72.27 ± 3.43	94.15 ± 4.23	33.02 ± 5.06	1.30 ± 0.09	0.46 ± 0.07
15	2.21 ± 0.55	–	–	–	–
16	–	–	13.52 ± 7.79	–	–
17	47.81 ± 3.10	46.82 ± 8.58	17.26 ± 9.04	0.98 ± 0.19	0.36 ± 0.19
18	32.37 ± 1.35	23.83 ± 3.59	21.13 ± 5.95	0.74 ± 0.12	0.65 ± 0.19
19	– nd	6.04 ± 0.71	12.25 ± 5.62	–	–
20	28.78 ± 1.44	25.20 ± 12.17	21.22 ± 9.69	0.88 ± 0.43	0.74 ± 0.34
BC5-B					
1	16.27 ± 0.96	–	11.06 ± 2.36	–	0.68
2	1.59 ± 0.57	–	–	–	–
3	133.05 ± 5.39	137.67 ± 2.57	66.62 ± 5.20	1.03 ± 0.05	0.50 ± 0.04
4	3.94 ± 0.92	–	7.64 ± 4.47	–	1.94 ± 1.22
5	121.04 ± 4.76	112.56 ± 5.94	48.20 ± 3.71	0.93 ± 0.06	0.40 ± 0.03
6	56.31 ± 2.46	71.14 ± 1.34	32.18 ± 2.73	1.26 ± 0.06	0.57 ± 0.05
7	92.59 ± 4.93	72.03 ± 2.26	39.36 ± 6.37	0.78 ± 0.05	0.43 ± 0.07
8	66.75 ± 2.68	49.73 ± 2.48	32.01 ± 7.68	0.75 ± 0.05	0.48 ± 0.12
9	42.96 ± 2.44	34.90 ± 2.33	20.46 ± 3.84	0.81 ± 0.07	0.48 ± 0.12
10	67.44 ± 3.33	46.37 ± 3.28	20.29 ± 4.37	0.69 ± 0.06	0.30 ± 0.07
11	13.16 ± 1.35	–	9.73 ± 3.26	–	0.74 ± 0.26
12	128.67 ± 5.75	120.94 ± 3.83	51.58 ± 3.69	0.94 ± 0.05	0.40 ± 0.03
13	7.28 ± 0.54	–	–	–	–
14	3.38 ± 0.81	–	4.94 ± 4.07	–	1.46 ± 1.26
15	1.34 ± 0.86	8.53 ± 5.56	–	6.38 ± 5.86	–
16	31.77 ± 1.72	21.92 ± 10.13	4.34 ± 3.24	0.69 ± 0.32	0.14 ± 0.10
17	55.00 ± 2.50	48.74 ± 3.61	29.34 ± 4.50	0.89 ± 0.08	0.53 ± 0.09
18	4.98 ± 0.91	–	5.53 ± 3.67	–	1.11 ± 0.76
19	110.85 ± 4.62	95.79 ± 2.73	38.85 ± 5.71	0.86 ± 0.04	0.35 ± 0.05
20	73.19 ± 3.34	57.58 ± 2.17	21.52 ± 6.97	0.79 ± 0.05	0.29 ± 0.10
BC5-C					
1	4.27 ± 0.46	–	–	–	–
2	1.39 ± 0.58	–	7.39 ± 6.63	–	5.31 ± 5.25
3	6.62 ± 0.66	6.00 ± 2.18	6.59 ± 3.36	0.91 ± 0.34	0.99 ± 0.52
4	4.15 ± 0.66	–	5.49 ± 3.27	–	1.32 ± 0.82
5	0.94 ± 0.78	–	6.68 ± 3.46	–	7.07 ± 6.87
6	20.52 ± 1.27	18.03 ± 3.37	–	0.88 ± 0.17	–
7	3.23 ± 0.97	–	8.05 ± 5.85	–	2.49 ± 1.96

Table 4 (*continued*)

Sample	Cl moles ($\times 10^{-12}$)	Br moles ($\times 10^{-15}$)	K moles ($\times 10^{-12}$)	Br/Cl ($\times 10^{-3}$)	K/Cl
BC5-A					
8	1.61 ± 0.64	–	32.41 ± 8.69	–	20.16 ± 9.71
9	11.05 ± 1.31	–	14.58 ± 6.20	–	1.32 ± 0.58
10	16.10 ± 1.13	7.99 ± 1.92	16.19 ± 3.02	0.50 ± 0.12	1.01 ± 0.20
11	10.58 ± 3.28	–	167.75 ± 11.05	–	15.85 ± 5.03

1.2×10^{-3} and 1.4×10^{-3} M, and are similar to the compositions measured in this study. The third sample had a significantly higher Br/Cl value in the range 1.70×10^{-3}–3.92×10^{-3} M with a mean of 2.5×10^{-3} M, interpreted as reflecting fractionation of a Cl bearing phase (Irwin and Roedder, 1995).

There is a good correlation between K and Cl in samples BC5-A and BC5-B with K/Cl values in the range 0.28–0.87 M, and average values of 0.37 and 0.42 M, respectively (Fig. 2). Fewer measurements were obtained on sample BC5-C but the data suggest K and Cl are less well-correlated. This sample was richest in K, with four out of five measurements recording K/Cl > 1. The K/Cl values are slightly higher than the value of ~ 0.25 M reported by Irwin and Roedder (1995) who attributed values > 0.3 M to the presence of relatively rare mica.

Problems were encountered during laser analysis due to limitations of the optical system and the detection limits as previously discussed. Using the present optical system, it was not possible to unambiguously identify individual fluid inclusions and daughter minerals at high magnification ($300\times$). The low abundance of I in the fluid and the relatively high blank level of ^{40}Ar precluded measurement of these two species using the laser technique. The problem of high detection limit for K was overcome by targeting groups of similar inclusions.

4.2. Bulk analysis of fluid inclusion populations

The Br/Cl and I/Cl data for Bingham Canyon quartz samples, obtained by in vacuo crushing and stepped heating are displayed in Fig. 3. The 'bulk' value is determined by summing the halogens released by both extraction techniques. The bulk values of Br/Cl = 1.16×10^{-3} M and I/Cl = 19.1×10^{-6} M provide reference points for comparing the effects of crushing and stepped heating.

The highest Br/Cl and I/Cl values (1.98×10^{-3} and 29.8×10^{-6} M, respectively) are obtained from the first crush of the samples. In subsequent crushes, the Br/Cl and I/Cl values decrease but do not reach those of the bulk values (Fig. 3). In contrast, the low temperature step gives the lowest Br/Cl and I/Cl ratios (0.15×10^{-3} and 2.66×10^{-6} M, respectively). At temperatures greater than 400°C, the halogen ratios increase until they are similar to the bulk values (Fig. 3). The variation in the Br/Cl and I/Cl is believed to reflect the selective release of noble gases from fluid and solid phases in the fluid inclusions. Br and I have low partition coefficients in halite leading to their enrichment in the fluid phase. Crushing will selectively release noble gases from the fluid phase leading to high Br/Cl and I/Cl values. Halite crystals have correspondingly low Br and I contents and are melted by heating giving much lower Br/Cl and I/Cl values. The increase in these ratios at high temperature indicates release from unbroken fluid inclusions in the crushed powder. The similarity between the average Br/Cl value determined by laser analysis (1.07×10^{-3} M) and that of the bulk value (1.16×10^{-3} M) indicates laser ablation releases noble gases from both the fluid and the solid halite daughter phases.

The Br/I correlation in Fig. 3 is referred to as the 'halite effect' (Cloke and Kesler, 1979). The Br/I value of ~ 50 is consistent with a higher compatibility of Br in halite compared with I. Assuming that the partition coefficients of Br and I are relatively insensitive to the presence of minor and trace elements, and given halite is the dominant Cl-bearing mineral within the inclusions, the Br/I ratio can be used to estimate the partition coefficient of I in

Table 5
Bingham Canyon, crush and step heating data

Sample	^{40}Ar mol ($\times 10^{-15}$)	^{36}Ar mol ($\times 10^{-15}$)	K mol ($\times 10^{-9}$)	Cl mol ($\times 10^{-9}$)	Br mol ($\times 10^{-12}$)	I mol ($\times 10^{-12}$)
BC5-A						
Crushing						
Crush 1	550.02 ± 7.09	0.98 ± 0.05	12.29 ± 0.23	45.96 ± 0.86	72.45 ± 1.56	1.18 ± 0.08
Crush 2	584.00 ± 7.44	0.94 ± 0.06	18.59 ± 0.38	68.98 ± 1.26	102.90 ± 2.38	1.62 ± 0.05
Crush 3	227.36 ± 2.66	0.31 ± 0.05	9.41 ± 0.20	36.07 ± 0.66	50.80 ± 1.04	0.81 ± 0.03
Crush 4	97.44 ± 0.58	0.08 ± 0.05	4.52 ± 0.08	17.90 ± 0.28	25.60 ± 0.52	0.40 ± 0.01
Heating						
200°C	393.24 ± 15.49	1.29 ± 0.06	0.97 ± 0.11	5.10 ± 0.21	0.78 ± 0.18	0.02 ± 0.01
400°C	628.95 ± 24.70	2.17 ± 0.10	14.88 ± 2.96	40.08 ± 1.70	17.15 ± 2.26	0.19 ± 0.01
600°C	1174.28 ± 45.72	4.15 ± 0.17	30.95 ± 1.35	25.33 ± 1.04	31.01 ± 4.08	0.27 ± 0.01
800°C	346.71 ± 13.38	1.09 ± 0.05	7.93 ± 0.35	7.74 ± 0.32	8.99 ± 1.17	0.14 ± 0.01
1000°C	332.71 ± 1.02	1.03 ± 0.06	3.69 ± 0.09	5.04 ± 0.08	5.53 ± 0.32	0.08 ± 0.01
1200°C	440.42 ± 1.38	1.23 ± 0.05	7.34 ± 0.14	23.11 ± 0.34	25.76 ± 1.56	–
1400°C	704.75 ± 4.12	1.99 ± 0.05	11.86 ± 0.17	41.05 ± 0.61	45.33 ± 2.76	0.06 ± 0.08
Total	5479.89 ± 57.03	15.27 ± 0.25	122.43 ± 3.32	316.37 ± 2.73	386.31 ± 6.54	4.78 ± 0.13
BC5-B						
Crushing						
Crush 1	1136.45 ± 14.42	2.78 ± 0.06	40.29 ± 0.76	137.63 ± 2.55	234.30 ± 12.62	3.83 ± 0.12
Crush 2	246.94 ± 1.33	0.59 ± 0.04	11.36 ± 0.20	40.18 ± 0.62	68.99 ± 1.50	1.20 ± 0.04
Crush 3	227.94 ± 1.21	0.40 ± 0.05	19.24 ± 0.33	69.26 ± 1.06	125.26 ± 2.61	2.21 ± 0.07
Crush 4	97.91 ± 0.52	0.14 ± 0.06	9.12 ± 0.20	34.06 ± 0.55	53.98 ± 1.42	0.91 ± 0.03
Heating						
400°C	299.28 ± 1.60	1.05 ± 0.07	6.68 ± 0.20	91.71 ± 1.43	30.78 ± 0.40	0.29 ± 0.02
600°C	1172.16 ± 7.91	4.44 ± 0.04	21.39 ± 0.32	46.67 ± 0.71	55.27 ± 1.26	0.81 ± 0.03
800°C	172.77 ± 1.33	0.62 ± 0.05	5.76 ± 0.20	10.14 ± 0.16	14.54 ± 0.19	0.25 ± 0.01
1000°C	196.88 ± 0.91	0.68 ± 0.03	4.20 ± 0.24	6.83 ± 0.12	7.50 ± 0.21	0.12 ± 0.00
1200°C	410.22 ± 2.05	1.22 ± 0.04	10.27 ± 0.17	35.18 ± 0.53	41.96 ± 1.14	0.62 ± 0.03
1400°C	672.99 ± 3.11	2.07 ± 0.05	12.34 ± 0.25	43.41 ± 0.72	52.06 ± 0.65	0.79 ± 0.03
Total	4633.55 ± 17.12	13.99 ± 0.16	140.66 ± 1.05	515.08 ± 3.42	684.63 ± 13.19	11.01 ± 0.15
BC5-C						
Crushing						
Crush 1	566.95 ± 3.17	1.35 ± 0.04	7.55 ± 0.16	24.98 ± 0.38	49.35 ± 1.02	0.74 ± 0.02
Crush 2	2235.16 ± 11.85	3.84 ± 0.04	69.53 ± 1.05	248.85 ± 3.81	213.45 ± 11.01	6.29 ± 0.20
Crush 3	570.52 ± 4.36	0.64 ± 0.07	25.54 ± 0.39	95.96 ± 1.49	155.74 ± 3.34	2.28 ± 0.07
Crush 4	407.22 ± 3.75	0.21 ± 0.04	20.35 ± 0.30	77.49 ± 1.23	125.49 ± 12.58	1.90 ± 0.06
Crush 5	396.96 ± 2.21	0.24 ± 0.05	21.65 ± 0.36	84.51 ± 1.30	125.14 ± 2.69	1.89 ± 0.06
Crush 6	154.27 ± 0.86	0.09 ± 0.06	9.31 ± 0.20	37.61 ± 0.57	51.44 ± 1.07	0.79 ± 0.02
Heating						
400°C	453.33 ± 2.12	1.47 ± 0.04	9.35 ± 0.27	157.49 ± 2.36	43.60 ± 1.51	0.42 ± 0.02
600°C	638.04 ± 1.67	1.85 ± 0.05	26.03 ± 0.41	66.59 ± 0.99	69.36 ± 1.65	0.95 ± 0.04
800°C	225.26 ± 1.10	0.68 ± 0.05	10.79 ± 0.33	13.38 ± 0.22	14.85 ± 0.43	0.23 ± 0.01
1000°C	178.33 ± 0.79	0.50 ± 0.04	4.25 ± 0.21	11.48 ± 0.18	11.81 ± 0.47	0.14 ± 0.01
1200°C	519.81 ± 4.71	0.89 ± 0.05	19.68 ± 0.29	76.50 ± 1.17	86.27 ± 2.25	1.37 ± 0.04
1400°C	568.13 ± 3.97	1.42 ± 0.05	15.70 ± 0.23	55.78 ± 0.84	51.94 ± 1.31	0.76 ± 0.02
Total	6914.00 ± 15.36	13.19 ± 0.17	239.74 ± 1.44	950.62 ± 5.39	998.43 ± 17.67	17.78 ± 0.24

Sample	^{40}Ar mol ($\times 10^{-15}$)	^{36}Ar mol ($\times 10^{-15}$)	K mol ($\times 10^{-9}$)	Cl mol ($\times 10^{-9}$)
BC4				
Crushing				
Crush 1	306.60 ± 3.68	0.58 ± 0.03	8.34 ± 0.16	2.34 ± 0.12
Crush 2	423.83 ± 5.07	0.56 ± 0.04	16.45 ± 0.31	4.02 ± 0.20

Table 5 (*continued*)

Sample	^{40}Ar mol ($\times 10^{-15}$)	^{36}Ar mol ($\times 10^{-15}$)	K mol ($\times 10^{-9}$)	Cl mol ($\times 10^{-9}$)
BC4				
Crushing				
Crush 3	247.62 ± 0.72	0.30 ± 0.02	13.44 ± 0.20	3.74 ± 0.13
Crush 4	209.29 ± 0.58	0.17 ± 0.04	15.45 ± 0.23	5.34 ± 0.09
Crush 5	224.67 ± 0.74	0.23 ± 0.05	18.99 ± 0.28	9.78 ± 0.15
Crush 6	76.04 ± 0.18	0.15 ± 0.04	5.54 ± 0.09	4.81 ± 0.08
Heating				
200°C	342.23 ± 0.55	1.32 ± 0.03	4.28 ± 0.06	12.68 ± 0.19
400°C	185.26 ± 0.26	0.55 ± 0.04	14.73 ± 0.22	93.54 ± 1.32
600°C	277.01 ± 0.41	0.81 ± 0.04	2.23 ± 0.03	250.05 ± 3.54
800°C	79.31 ± 1.75	0.20 ± 0.03	2.17 ± 0.05	48.05 ± 0.69
1000°C	125.07 ± 0.41	0.47 ± 0.05	2.93 ± 0.06	16.01 ± 0.35
1200°C	281.79 ± 0.89	0.57 ± 0.04	17.59 ± 0.26	15.88 ± 0.24
1400°C	233.36 ± 0.74	0.61 ± 0.03	11.30 ± 0.18	9.10 ± 0.22
1600°C	448.24 ± 1.43	1.52 ± 0.03	2.53 ± 0.04	1.64 ± 0.11
Total	3460.32 ± 6.91	8.04 ± 0.14	135.97 ± 0.68	476.97 ± 3.89
BC3				
Crushing				
Crush 1	18.91 ± 0.07	0.10 ± 0.03	0.70 ± 0.05	0.98 ± 0.03
Crush 2	99.96 ± 0.27	0.23 ± 0.04	7.58 ± 0.13	7.97 ± 0.12
Crush 3	157.64 ± 0.46	0.34 ± 0.04	13.62 ± 0.31	15.26 ± 0.23
Crush 4	145.51 ± 0.45	0.23 ± 0.05	27.12 ± 0.41	15.44 ± 0.23
Crush 5	82.81 ± 0.99	0.19 ± 0.03	28.29 ± 0.55	8.39 ± 0.16
Crush 6	84.39 ± 1.02	0.18 ± 0.03	39.50 ± 0.78	8.43 ± 0.17
Heating				
200°C	158.90 ± 0.51	0.55 ± 0.04	120.87 ± 1.75	6.79 ± 0.11
400°C	436.17 ± 1.70	0.77 ± 0.06	912.91 ± 13.08	15.02 ± 0.24
600°C	837.56 ± 2.05	0.25 ± 0.04	3103.69 ± 44.34	1.85 ± 0.03
800°C	155.79 ± 0.45	0.22 ± 0.08	452.97 ± 6.48	1.99 ± 0.09
1000°C	105.08 ± 0.25	0.25 ± 0.03	171.25 ± 2.45	3.22 ± 0.06
1200°C	119.86 ± 0.30	0.28 ± 0.04	51.76 ± 0.74	11.41 ± 0.17
1400°C	129.62 ± 0.31	0.45 ± 0.05	7.03 ± 0.11	8.31 ± 0.13
1600°C	355.25 ± 0.86	1.29 ± 0.05	1.10 ± 0.04	2.05 ± 0.03
Total	2887.46 ± 3.32	5.32 ± 0.17	4938.38 ± 46.79	107.12 ± 0.55
BC2				
Crushing				
Crush 1	284.93 ± 0.81	0.98 ± 0.04	5.07 ± 0.09	0.63 ± 0.02
Crush 2	352.40 ± 1.26	1.15 ± 0.06	9.68 ± 0.17	0.88 ± 0.03
Crush 3	651.32 ± 3.71	2.03 ± 0.03	32.47 ± 0.51	2.77 ± 0.05
Crush 4	498.31 ± 4.21	1.56 ± 0.05	80.84 ± 1.28	4.10 ± 0.08
Crush 5	289.58 ± 1.70	0.83 ± 0.04	120.62 ± 1.84	3.59 ± 0.06
Crush 6	156.93 ± 0.89	0.44 ± 0.03	115.53 ± 1.75	2.20 ± 0.04
Crush 7	50.22 ± 0.13	0.17 ± 0.04	53.06 ± 0.77	0.77 ± 0.02
Heating				
200°C	270.77 ± 0.59	0.44 ± 0.04	576.13 ± 8.11	0.61 ± 0.05
400°C	1170.30 ± 0.85	0.72 ± 0.04	3733.22 ± 52.61	2.31 ± 0.04
600°C	3570.05 ± 3.80	0.85 ± 0.06	13391.64 ± 188.91	8.43 ± 0.15
800°C	637.15 ± 0.45	0.38 ± 0.02	2303.33 ± 32.43	6.65 ± 0.11
1000°C	346.01 ± 0.30	0.33 ± 0.03	948.79 ± 13.37	7.09 ± 0.10
1200°C	91.31 ± 0.13	0.29 ± 0.04	54.10 ± 0.76	2.68 ± 0.05

(continued on next page)

Table 5 (*continued*)

Sample	^{40}Ar mol ($\times 10^{-15}$)	^{36}Ar mol ($\times 10^{-15}$)	K mol ($\times 10^{-9}$)	Cl mol ($\times 10^{-9}$)
BC2				
Heating				
1400°C	100.43 ± 0.07	0.40 ± 0.04	6.39 ± 0.22	1.33 ± 0.02
1600°C	297.27 ± 0.25	1.10 ± 0.02	1.21 ± 0.07	0.07 ± 0.02
Total	8766.98 ± 7.30	11.67 ± 0.15	21432.10 ± 199.40	44.11 ± 0.26
SB8				
Crushing				
Crush 1	332.29 ± 0.94	0.39 ± 0.03	9.28 ± 0.14	7.01 ± 0.11
Crush 2	286.17 ± 0.76	0.28 ± 0.05	11.18 ± 0.19	6.14 ± 0.09
Crush 3	271.92 ± 0.84	0.45 ± 0.05	7.40 ± 0.24	4.66 ± 0.07
Crush 4	475.77 ± 1.17	0.41 ± 0.04	46.63 ± 0.75	11.26 ± 0.17
Crush 5	320.53 ± 0.87	0.28 ± 0.03	45.31 ± 0.65	7.38 ± 0.12
Heating				
200°C	346.87 ± 11.16	1.16 ± 0.04	30.52 ± 0.49	0.21 ± 0.02
400°C	507.40 ± 5.33	0.85 ± 0.04	323.51 ± 5.49	6.48 ± 0.11
600°C	1297.34 ± 11.05	0.86 ± 0.05	2623.72 ± 41.97	4.46 ± 0.10
800°C	622.50 ± 5.41	0.39 ± 0.07	1341.65 ± 21.50	0.96 ± 0.04
1000°C	678.90 ± 8.19	0.49 ± 0.03	1459.86 ± 22.40	1.76 ± 0.06
1200°C	1525.50 ± 8.68	0.77 ± 0.04	2647.27 ± 40.92	12.95 ± 0.22
1400°C	374.49 ± 2.84	0.52 ± 0.05	15.30 ± 0.73	9.26 ± 0.15
1600°C	314.10 ± 2.82	0.88 ± 0.05	1.55 ± 0.09	3.04 ± 0.06
Total	7353.78 ± 21.61	7.73 ± 0.16	8563.19 ± 66.58	75.58 ± 0.41
SB6				
Crushing				
Crush 1	522.24 ± 1.06	1.42 ± 0.04	1.52 ± 0.16	5.96 ± 0.09
Crush 2	372.10 ± 0.81	0.75 ± 0.07	1.12 ± 0.18	8.57 ± 0.13
Crush 3	334.37 ± 0.67	0.68 ± 0.06	0.93 ± 0.08	8.21 ± 0.12
Crush 4	266.33 ± 0.86	0.52 ± 0.04	1.03 ± 0.12	7.68 ± 0.12
Crush 5	241.79 ± 0.52	0.40 ± 0.06	1.20 ± 0.14	7.50 ± 0.13
Heating				
200°C	454.56 ± 19.05	1.52 ± 0.06	0.74 ± 0.27	0.15 ± 0.03
400°C	381.78 ± 4.92	1.14 ± 0.05	3.02 ± 0.24	2.92 ± 0.06
600°C	280.61 ± 9.77	0.80 ± 0.01	12.38 ± 0.34	1.55 ± 0.04
800°C	102.89 ± 1.16	0.29 ± 0.03	4.75 ± 0.16	0.46 ± 0.03
1000°C	105.72 ± 1.06	0.29 ± 0.03	2.30 ± 0.08	1.19 ± 0.05
1200°C	447.84 ± 6.04	0.69 ± 0.06	3.66 ± 0.15	12.76 ± 0.23
1400°C	430.41 ± 5.54	0.70 ± 0.03	3.89 ± 0.24	10.53 ± 0.19
1600°C	616.10 ± 8.84	1.31 ± 0.06	4.06 ± 0.24	12.21 ± 0.24
Total	4556.74 ± 25.17	10.50 ± 0.17	40.61 ± 0.71	79.70 ± 0.48
SB4				
Crushing				
Crush 1	1808.85 ± 4.84	5.36 ± 0.05	6.25 ± 0.33	11.95 ± 0.18
Crush 2	966.97 ± 2.65	2.84 ± 0.06	4.37 ± 0.30	7.53 ± 0.13
Crush 3	1028.90 ± 2.57	2.76 ± 0.05	7.64 ± 0.19	11.23 ± 0.17
Crush 4	444.48 ± 1.16	1.12 ± 0.04	6.17 ± 0.20	6.08 ± 0.12
Heating				
200°C	556.99 ± 7.63	2.03 ± 0.06	2.04 ± 0.19	0.51 ± 0.09
400°C	899.41 ± 31.12	2.24 ± 0.09	40.70 ± 1.46	9.59 ± 0.38
600°C	710.87 ± 23.84	1.55 ± 0.07	332.72 ± 12.52	4.28 ± 0.16
800°C	248.12 ± 0.73	0.44 ± 0.01	307.01 ± 4.43	0.53 ± 0.03
1000°C	122.83 ± 0.41	0.33 ± 0.02	48.14 ± 0.80	1.20 ± 0.05

Table 5 (*continued*)

Sample	^{40}Ar mol ($\times 10^{-15}$)	^{36}Ar mol ($\times 10^{-15}$)	K mol ($\times 10^{-9}$)	Cl mol ($\times 10^{-9}$)
SB4				
Heating				
1200°C	536.92 ± 2.26	1.16 ± 0.05	32.61 ± 0.47	10.65 ± 0.16
1400°C	1033.39 ± 3.71	2.01 ± 0.02	56.57 ± 0.83	25.34 ± 0.37
1600°C	469.64 ± 3.16	1.11 ± 0.05	12.38 ± 0.22	8.73 ± 0.13
Total	8827.36 ± 40.78	22.98 ± 0.18	856.59 ± 13.43	97.63 ± 0.68
SB1				
Crushing				
Crush 1	264.83 ± 0.52	0.77 ± 0.04	40.66 ± 0.60	1.93 ± 0.03
Crush 2	1025.72 ± 3.24	3.30 ± 0.06	21.67 ± 0.33	3.36 ± 0.05
Crush 3	681.33 ± 1.13	2.24 ± 0.05	22.12 ± 0.35	2.61 ± 0.05
Crush 4	595.90 ± 0.90	1.92 ± 0.04	22.50 ± 0.42	2.32 ± 0.08
Crush 5	338.12 ± 0.56	1.06 ± 0.06	20.66 ± 0.30	2.15 ± 0.05
Crush 6	239.98 ± 0.60	0.74 ± 0.04	26.09 ± 0.41	1.70 ± 0.04
Heating				
200°C	1363.31 ± 13.72	4.56 ± 0.03	62.37 ± 0.92	0.32 ± 0.02
400°C	1863.79 ± 8.56	5.33 ± 0.05	578.18 ± 8.34	3.84 ± 0.06
600°C	1728.57 ± 6.01	1.59 ± 0.05	2677.54 ± 39.50	3.54 ± 0.06
800°C	704.08 ± 2.90	0.34 ± 0.04	1358.76 ± 19.71	1.65 ± 0.04
1000°C	197.79 ± 0.90	0.35 ± 0.06	207.81 ± 3.00	1.66 ± 0.03
1200°C	407.18 ± 1.37	1.04 ± 0.04	25.04 ± 0.39	8.53 ± 0.13
1400°C	598.58 ± 1.09	2.39 ± 0.04	23.51 ± 0.34	11.10 ± 0.16
1600°C	345.73 ± 2.99	1.07 ± 0.05	4.57 ± 0.13	4.47 ± 0.07
Total	10354.9 ± 18.24	26.70 ± 0.17	5091.48 ± 45.05	49.17 ± 0.28
GM4				
Crushing				
Crush 1	3395.38 ± 7.63	9.18 ± 0.06	106.18 ± 1.54	46.38 ± 0.68
Crush 2	893.22 ± 2.06	1.66 ± 0.03	136.37 ± 1.95	30.42 ± 0.46
Crush 3	384.89 ± 0.96	0.74 ± 0.05	94.67 ± 1.36	13.35 ± 0.20
Crush 4	372.25 ± 0.85	0.48 ± 0.05	127.09 ± 1.86	14.36 ± 0.22
Crush 5	95.37 ± 1.41	0.09 ± 0.05	58.57 ± 0.86	3.83 ± 0.10
Heating				
200°C	263.26 ± 0.63	0.79 ± 0.05	105.63 ± 1.51	0.67 ± 0.01
400°C	573.80 ± 1.53	0.48 ± 0.03	628.45 ± 8.96	9.88 ± 0.15
600°C	1979.81 ± 8.60	1.02 ± 0.04	3722.13 ± 53.28	6.00 ± 0.09
800°C	2396.12 ± 20.20	0.40 ± 0.04	5348.40 ± 77.37	1.35 ± 0.07
1000°C	825.69 ± 2.66	0.20 ± 0.03	1767.13 ± 25.14	1.81 ± 0.05
1200°C	191.94 ± 1.50	0.29 ± 0.04	80.61 ± 1.14	8.42 ± 0.13
1400°C	180.35 ± 1.03	0.32 ± 0.04	6.48 ± 0.13	11.26 ± 0.18
1600°C	114.87 ± 0.40	0.35 ± 0.03	1.44 ± 0.17	4.33 ± 0.07
Total	11666.96 ± 23.69	15.99 ± 0.15	12183.16 ± 97.74	152.06 ± 0.93
GM3				
Crushing				
Crush 1	1262.90 ± 2.20	2.49 ± 0.04	3.52 ± 0.32	9.26 ± 0.15
Crush 2	822.84 ± 1.81	1.15 ± 0.05	2.78 ± 0.21	7.69 ± 0.13
Crush 3	773.32 ± 1.48	0.94 ± 0.05	5.32 ± 0.09	8.31 ± 0.13
Crush 4	245.54 ± 0.50	0.33 ± 0.06	4.11 ± 0.13	2.74 ± 0.06
Heating				
200°C	68.47 ± 0.92	0.27 ± 0.04	1.00 ± 0.10	0.13 ± 0.02
400°C	193.07 ± 0.93	0.34 ± 0.02	7.03 ± 0.13	1.54 ± 0.04

(*continued on next page*)

Table 5 (*continued*)

Sample	^{40}Ar mol ($\times 10^{-15}$)	^{36}Ar mol ($\times 10^{-15}$)	K mol ($\times 10^{-9}$)	Cl mol ($\times 10^{-9}$)
GM3				
Heating				
600°C	306.74 ± 1.67	0.68 ± 0.05	78.60 ± 1.17	1.36 ± 0.04
800°C	127.49 ± 0.58	0.25 ± 0.04	138.64 ± 2.07	0.16 ± 0.03
1000°C	93.71 ± 0.45	0.28 ± 0.05	38.20 ± 0.60	0.24 ± 0.02
1200°C	236.55 ± 0.26	0.38 ± 0.02	3.82 ± 0.11	2.06 ± 0.03
1400°C	172.27 ± 0.40	0.30 ± 0.04	1.85 ± 0.11	1.44 ± 0.04
1600°C	298.73 ± 0.75	0.71 ± 0.04	1.11 ± 0.08	1.86 ± 0.03
Total	4601.62 ± 4.05	8.11 ± 0.15	285.99 ± 2.50	36.80 ± 0.26
PV6				
Crushing				
Crush 1	1902.79 ± 5.20	2.01 ± 0.04	3.51 ± 0.16	6.16 ± 0.09
Crush 2	1047.13 ± 3.24	0.59 ± 0.06	4.54 ± 0.20	3.97 ± 0.07
Crush 3	419.86 ± 1.15	0.20 ± 0.03	3.65 ± 0.17	1.49 ± 0.04
Crush 4	688.70 ± 1.90	0.21 ± 0.06	7.34 ± 0.15	2.48 ± 0.04
Crush 5	143.70 ± 0.42	0.06 ± 0.05	2.15 ± 0.16	0.53 ± 0.04
Heating				
200°C	159.66 ± 1.48	0.50 ± 0.02	2.22 ± 0.19	0.06 ± 0.05
400°C	455.25 ± 1.69	0.39 ± 0.05	16.06 ± 0.25	1.33 ± 0.04
600°C	461.72 ± 1.20	0.34 ± 0.04	97.11 ± 1.39	1.27 ± 0.02
800°C	345.97 ± 1.13	0.86 ± 0.04	207.12 ± 2.95	0.10 ± 0.03
1000°C	71.58 ± 11.93	0.15 ± 0.03	61.05 ± 4.81	0.18 ± 0.02
1200°C	362.63 ± 14.76	0.34 ± 0.04	12.20 ± 0.38	1.03 ± 0.04
1400°C	456.49 ± 6.00	0.51 ± 0.05	2.45 ± 0.08	0.88 ± 0.03
1600°C	527.40 ± 6.60	1.15 ± 0.04	1.01 ± 0.13	0.80 ± 0.03
Total	7042.87 ± 22.13	7.31 ± 0.16	420.43 ± 5.84	20.28 ± 0.16
PV1				
Crushing				
Crush 1	2198.67 ± 5.84	5.48 ± 0.06	1.16 ± 0.13	3.14 ± 0.05
Crush 2	1117.25 ± 2.30	2.18 ± 0.05	1.81 ± 0.11	3.21 ± 0.06
Crush 3	529.71 ± 1.20	0.71 ± 0.04	1.83 ± 0.09	2.09 ± 0.04
Crush 4	493.06 ± 1.02	0.50 ± 0.05	3.77 ± 0.16	2.42 ± 0.06
Heating				
200°C	85.91 ± 1.16	0.27 ± 0.03	1.43 ± 0.11	0.14 ± 0.03
400°C	283.55 ± 42.37	0.07 ± 0.05	3.42 ± 0.73	2.20 ± 0.24
600°C	404.35 ± 5.17	0.61 ± 0.04	47.56 ± 2.07	0.72 ± 0.16
800°C	197.98 ± 12.80	0.30 ± 0.03	218.83 ± 3.58	0.14 ± 0.02
1000°C	95.03 ± 0.57	0.13 ± 0.03	76.59 ± 1.40	0.12 ± 0.02
1200°C	356.80 ± 7.15	0.44 ± 0.04	5.50 ± 0.14	1.57 ± 0.04
1400°C	285.25 ± 10.34	0.33 ± 0.05	1.47 ± 0.10	0.97 ± 0.04
1600°C	572.36 ± 11.59	0.92 ± 0.04	1.61 ± 0.22	1.72 ± 0.05
Total	6619.91 ± 48.18	11.94 ± 0.15	364.96 ± 4.44	18.43 ± 0.32
R3				
Crushing				
Crush 1	2006.29 ± 3.93	5.58 ± 0.05	17.18 ± 0.28	7.75 ± 0.12
Crush 2	773.39 ± 1.17	1.92 ± 0.06	19.05 ± 0.28	4.89 ± 0.08
Crush 3	769.98 ± 1.60	1.74 ± 0.05	34.74 ± 0.52	5.84 ± 0.10
Crush 4	666.89 ± 1.12	1.53 ± 0.05	37.44 ± 0.60	4.93 ± 0.09
Crush 5	1395.88 ± 2.25	4.14 ± 0.04	45.82 ± 0.72	3.72 ± 0.09
Crush 6	810.79 ± 2.04	1.74 ± 0.05	134.40 ± 1.91	5.40 ± 0.08
Crush 7	39.96 ± 0.13	0.00 ± 0.06	17.33 ± 0.38	

Table 5 (*continued*)

Sample	^{40}Ar mol ($\times 10^{-15}$)	^{36}Ar mol ($\times 10^{-15}$)	K mol ($\times 10^{-9}$)	Cl mol ($\times 10^{-9}$)
R3				
Heating				
200°C	127.45 ± 0.14	0.39 ± 0.03	33.78 ± 0.49	0.09 ± 0.02
400°C	407.87 ± 0.66	0.54 ± 0.03	323.76 ± 4.57	2.43 ± 0.04
600°C	1580.55 ± 8.42	1.13 ± 0.02	2543.75 ± 35.95	2.13 ± 0.05
800°C	647.53 ± 0.73	0.18 ± 0.04	1322.72 ± 18.66	0.26 ± 0.03
1000°C	112.61 ± 0.12	0.19 ± 0.03	105.01 ± 1.51	0.61 ± 0.01
1200°C	493.08 ± 1.06	0.84 ± 0.02	26.64 ± 0.38	5.52 ± 0.08
1400°C	564.48 ± 0.55	0.96 ± 0.03	26.44 ± 0.38	6.54 ± 0.10
1600°C	356.53 ± 0.73	0.74 ± 0.04	5.14 ± 0.12	3.14 ± 0.05
Total	10753.28 ± 10.18	21.63 ± 0.16	4693.22 ± 40.86	53.27 ± 0.28
R1				
Crushing				
Crush 1	1834.64 ± 10.02	4.50 ± 0.04	13.68 ± 0.29	36.19 ± 0.54
Crush 2	–	–	–	–
Crush 3	656.86 ± 1.08	1.08 ± 0.03	28.34 ± 0.42	28.76 ± 0.42
Crush 4	524.23 ± 0.89	0.75 ± 0.04	42.07 ± 0.64	25.55 ± 0.38
Crush 5	175.30 ± 0.25	0.24 ± 0.05	25.22 ± 0.40	9.02 ± 0.14
Heating				
200°C	265.07 ± 0.39	0.84 ± 0.01	38.63 ± 0.55	0.76 ± 0.03
400°C	470.74 ± 0.40	0.81 ± 0.04	244.59 ± 3.45	9.30 ± 0.14
600°C	1409.26 ± 1.76	0.96 ± 0.03	2401.19 ± 33.84	7.29 ± 0.11
800°C	922.40 ± 1.16	0.23 ± 0.04	1896.44 ± 26.74	1.33 ± 0.03
1000°C	350.52 ± 0.53	0.21 ± 0.03	640.54 ± 9.04	1.43 ± 0.03
1200°C	910.10 ± 1.22	0.92 ± 0.04	1171.56 ± 16.49	17.10 ± 0.25
1400°C	316.94 ± 0.12	0.71 ± 0.04	38.40 ± 0.56	17.05 ± 0.25
1600°C	287.95 ± 0.38	0.78 ± 0.05	4.85 ± 0.15	8.81 ± 0.13
Total	8124.00 ± 10.44	12.03 ± 0.13	6545.50 ± 47.19	162.61 ± 0.90

halite. A recent estimate of the average Br partition coefficient in halite of 0.033 (Siemann and Schramm, 2000) would suggest that the partition coefficient for I is < 0.001, which is broadly similar to previous estimates (Holser, 1979)

4.2.1. K/Cl

Potassium and Cl measured by in vacuo crushing show a good correlation with a K/Cl value of 0.30 M (Fig. 4), lower than that obtained during laser analysis (0.37 and 0.42 M). The K/Cl measured during stepped heating is more variable than that measured by the other techniques and tends to be higher. Of the three samples from the BC5 vein, two values of > 1 have been determined; among the remaining Bingham Canyon and Arizonan samples, many values of K/Cl > 1 have been recorded (Table 1). The different values determined by the three techniques reflect the fact that K is located in solid phases. Data obtained by in vacuo crushing, which samples fluid phases and typically releases only ~ 5% of a samples total K, has a uniform but low K/Cl ratio. Data obtained by step heating, which releases as much as ~ 95% of a samples total K, has the highest K/Cl ratio often exceeding one, and suggesting the presence of mica or K-feldspar. The fact that K/Cl ratios obtained by laser analysis are intermediate to those of in vacuo crushing and step heating is compatible with laser ablation sampling noble gases from both solid and fluid phases.

4.3. Implications for bulk fluid inclusion analyses

Daughter minerals such as halite fractionate halogens, therefore the halogen composition of the original fluid cannot be determined by crushing experiments alone. In order to obtain reliable halogen compositions, stepped heating of samples is required

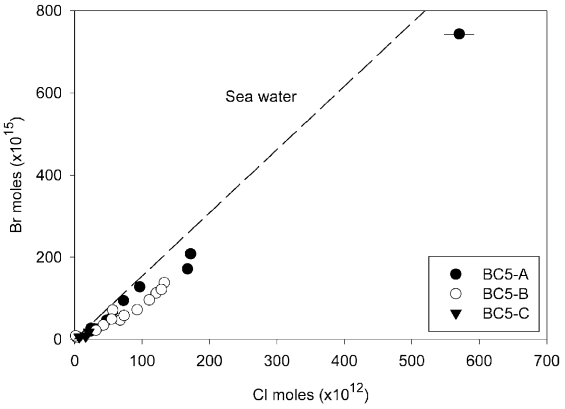

Fig. 1. Plot of Br and Cl data obtained by laser analysis of the three Bingham Canyon samples BC5-A, BC5-B and BC5-C. The Br/Cl of seawater is shown for reference, although the fluid inclusions show considerable variability all have a Br/Cl ratio of less than seawater.

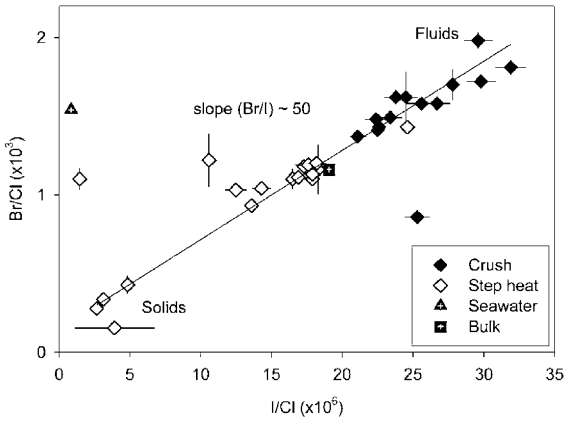

Fig. 3. Halogen plot for the Bingham Canyon sample BC5. This data demonstrates the complimentary nature of the two bulk extraction techniques. In vacuo crushing mechanically opens inclusions releasing fluid phases rich in the incompatible Br and I ions. Step heating allows diffusion of gas from solid phases such as halite, which contain mainly Cl.

to obtain bulk values. However, it should be emphasised that halite does not incorporate significant quantities of the noble gases and hence does not fractionate the isotopic or elemental ratios of natural noble gases within the fluid. The initial noble gas composition of fluids can therefore be reliably studied from the crushing data. Moreover, crushing has the advantage that, because K is often concentrated within solid K-bearing daughter phases or syngenetic mica, very little $^{39}Ar_K$ or radiogenic ^{40}Ar ($^{40}Ar_R$) is released and so corrections for in situ $^{40}Ar_R$ produced since trapping are small. This enables data from crushing to be used to reliably estimate amounts of $^{40}Ar_E$ in the fluid and the initial $^{40}Ar/^{36}Ar$ ratio.

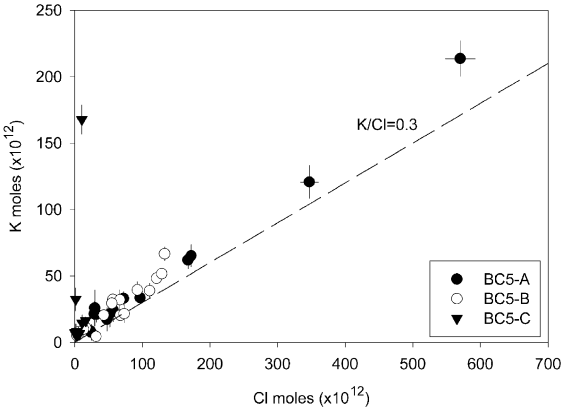

Fig. 2. Plot of K and Cl data obtained by laser analysis of the three Bingham Canyon samples BC5-A, BC5-B and BC5-C. The K/Cl ratio measured by laser analysis is slightly higher than that measured in-vacuo crushing, see text (Fig. 4).

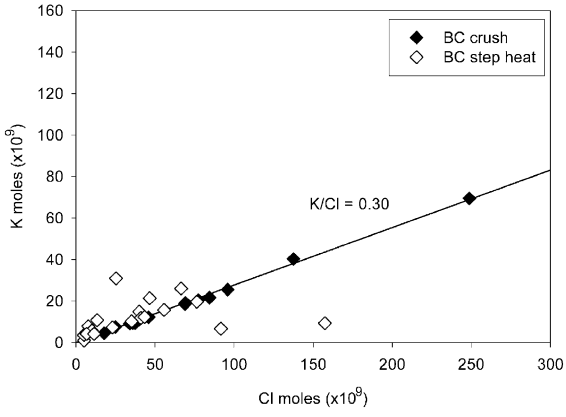

Fig. 4. K and Cl plot for the Bingham Canyon sample BC5. Data obtained from the fluids by in vacuo crushing is well correlated with an average K/Cl of 0.3. Step heating of the crushed residue, which preferentially samples solid phases, has a variable K/Cl ratio, dependent on the amount of K released from solid phases in each step. With the exception of two points, the step heating data lies on or above the correlation measured during in vacuo crushing.

4.3.1. Combined noble gas and halogen plots

It is useful to plot $^{40}Ar/^{36}Ar$ against $Cl/^{36}Ar$ for the purposes of comparing Ar data between samples (Bohlke and Irwin, 1992c; Irwin and Reynolds, 1995; Irwin and Roedder, 1995; Turner and Bannon, 1992). The correlation between Cl and $^{40}Ar_E$ is interpreted as a mixing line between a 'primary' brine component, rich in Cl and containing $^{40}Ar_E$, and a low salinity component consisting of meteoric water (containing atmospheric Ar) and air (Fig. 5).

The $^{40}Ar_E/Cl$ ratio has been used in previous studies to fingerprint the source of a mineralising fluid and the extent of interaction with country rock (Turner and Bannon, 1992). Comparison of $^{40}Ar_E/Cl$ determined by both crushing and step heating show that differences in the ratios are usually within a factor of 1.5 (Table 5). This is not surprising since, averaged over the fluid inclusion population, comparatively little of the total Cl in the sample is in the form of halite (average salinity < 17 wt.% NaCl equiv.). An additional advantage is that in most cases data obtained by in vacuo crushing does not require correction for $^{40}Ar_R$ (Table 6). Furthermore, since the actual $^{40}Ar_E/Cl$ ratios in the porphyry fluids vary by orders of magnitude (Fig. 5), it seems justified to base interpretations on noble gas and Cl ratios on data determined through in vacuo crushing alone.

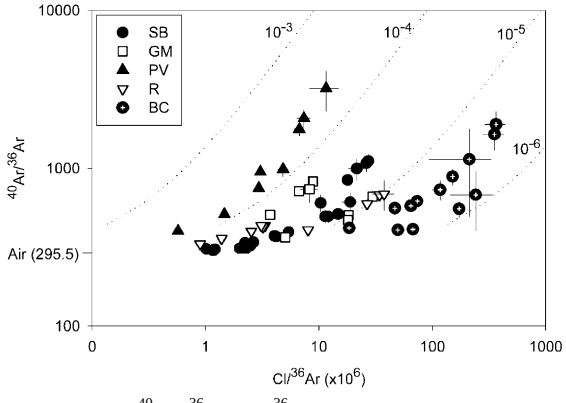

Fig. 5. Plot of $^{40}Ar/^{36}Ar$–$Cl/^{36}Ar$ for all the deposits studied, trajectories of the $^{40}Ar_E/Cl$ ratio have been plotted with an intercept of 295 and appear as parabolas in log–log space. The data was obtained by in vacuo crushing analysis which releases very little $^{40}Ar_R$, consequently the diagram is equivalent to a diagram that has been corrected for $^{40}Ar_R$ produced since fluid trapping. Data from each deposit falls on a binary mixing array between a low salinity meteoric component containing air and a high salinity brine component. The slope, $^{40}Ar_E/Cl$ varies by orders of magnitude from $> 10^{-4}$ at Pinto Valley to $\sim 10^{-6}$ at Bingham Canyon.

Table 6
Comparison of $^{40}Ar_E/Cl$ ratios obtained by in vacuo crushing, corrected and uncorrected for $^{40}Ar_R$[a]

Sample	GM4	GM3	R3	R1	BC5-A	BC5-B	BC5-C
Uncorrected ($\times 10^{-5}$)	1.9	5.8	4.7	1.1	0.4	0.2	0.4
$^{40}Ar_R$ corrected ($\times 10^{-5}$)	1.2	5.7	4.1	1.0	0.4	0.1	0.4

Sample	SB8	SB6	SB4	SB1	PV6	PV1
Uncorrected ($\times 10^{-5}$)	3.3	1.6	1.9	1.9	26.6	14.0
$^{40}Ar_R$ corrected ($\times 10^{-5}$)	3.0	1.6	1.9	1.0	26.5	13.9

[a] $^{40}Ar_E/Cl$ ratios are representative of each sample and obtained from the slope of data in $^{40}Ar/^{36}Ar$ vs. $Cl/^{36}Ar$ plots such as Fig. 5. The small effect of the $^{40}Ar_R$ correction reflects the fact that very little $^{39}Ar_K$ or $^{40}Ar_R$ is released by in vacuo crushing.

5. Age of mineralisation determined using ^{40}Ar–^{36}Ar–K–Cl mixing diagrams

The combined use of crushing and step heating data provides a method for Ar–Ar age determinations that incorporates a correction for $^{40}Ar_E$. Accurate and meaningful ages of ore deposition can be obtained because quartz veins host the mineralisation, and therefore it is possible to avoid the assumptions inherent in isotopic dating of host rock alteration minerals.

Disentangling different ^{40}Ar components (air—$^{40}Ar_A$; $^{40}Ar_R$ and $^{40}Ar_E$) of fluid inclusions can be achieved using correlations involving ^{40}Ar, ^{36}Ar, Cl and K (Kelley et al., 1986; Turner, 1988; Turner and Bannon, 1992). Potassium and $^{40}Ar_R$ in fluid inclusions are sited predominantly in K-bearing daughter minerals (e.g. sylvite) and syngenetic mica or feldspar. Only minor amounts of these K-derived components are released by in vacuo crushing compared with stepped heating. On a plot of $K/^{36}Ar$, $Cl/^{36}Ar$ and $^{40}Ar/^{36}Ar$, the position of each data point is determined by the proportions of the three ^{40}Ar end-member components that are present: air

($^{40}Ar_A$ and ^{36}Ar), fluid (rich in Cl and $^{40}Ar_E$) and solid (rich in K and $^{40}Ar_R$).

Crushing preferentially releases noble gases from fluid, essentially a binary mixing between fluid and air and the data are aligned along the edge of a plane defined by $^{40}Ar/^{36}Ar$ and $Cl/^{36}Ar$ (Fig. 6). Stepped heating preferentially releases $^{40}Ar_R$ and $^{39}Ar_K$ from solids and some Ar from fluid and air in remaining undecrepitated fluid inclusions. The step heating data therefore has relatively high $K/^{36}Ar$ and low $Cl/^{36}Ar$ values, but K/Cl is variable and the points lie on a plane (Fig. 6). The orientations of the fitted planes reflect the abundance of K bearing phases (Table 1) and the relative contributions of $^{40}Ar_E$ and $^{40}Ar_R$: Pinto Valley which has $< 0.3\%$ mica inclusions is dominated by Cl-correlated $^{40}Ar_E$; Ray and Globe-Miami contain up to $\sim 8\%$ mica inclusions and are dominated by K-correlated $^{40}Ar_R$. The Silverbell samples are variable containing between $< 0.1\%$ and 7% mica inclusions in addition to significant $^{40}Ar_E$, because of this the orientation of the plane is intermediate to those of the other deposits. Bingham Canyon samples BC5 and BC4 from the potassic zone are dominated by $^{40}Ar_E$ while sample BC2 from the propylitic zone, and to a lesser extent sample BC3 from the potassic zone, are rich in mica inclusions and dominated by $^{40}Ar_R$ (Fig. 7a).

Projection of the plane onto the $^{40}Ar/^{36}Ar$ and $Cl/^{36}Ar$ axes defines the correlation between Cl and $^{40}Ar_E$ (Fig. 5) and enables a $^{40}Ar_E/Cl$ ratio to be obtained (Table 6). Intersection of the plane with the $^{40}Ar/^{36}Ar$ and $K/^{36}Ar$ axes defines a correlation

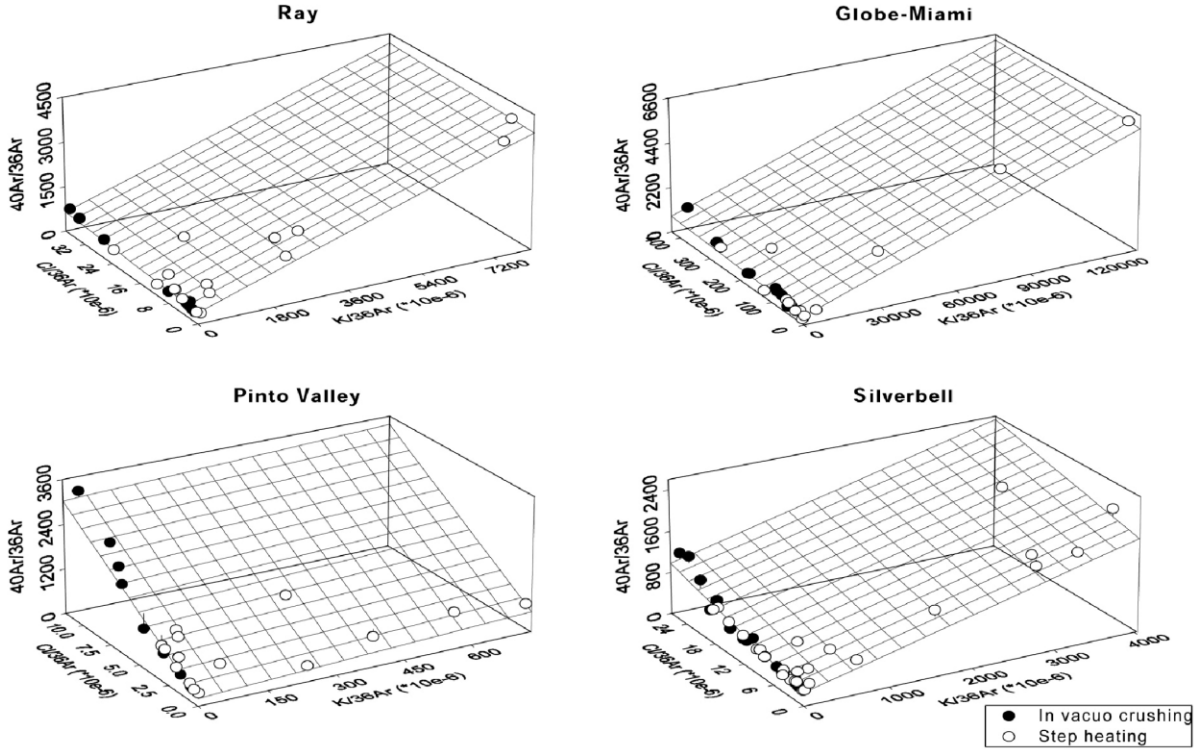

Fig. 6. Multi-isotope, $^{40}Ar–^{36}Ar–K–Cl$, 3D correlation diagrams for Silverbell, Globe Miami, Pinto Valley and Ray. The data at each deposit lies on a plane representing a mixture of three endmember components; air, fluid and solid (see text). The orientation of the plane depends on the balance of $^{40}Ar_E$, Cl, K and $^{40}Ar_R$, drop lines connect outlying data points with the plane demonstrating the good fit of the data. Each plot is orientated with air ($^{40}Ar/^{36}Ar = 296$) at the front corner, data obtained by in vacuo crushing lies along the $Cl/^{36}Ar$ axis, and data obtained by step heating has variable K/Cl, and higher $K/^{36}Ar$ lies on the plane. Projection of the plane onto the $^{40}Ar/^{36}Ar–K/^{36}Ar$ axis, enables determination of the $^{40}Ar_R/K$ ratio, and thus the age.

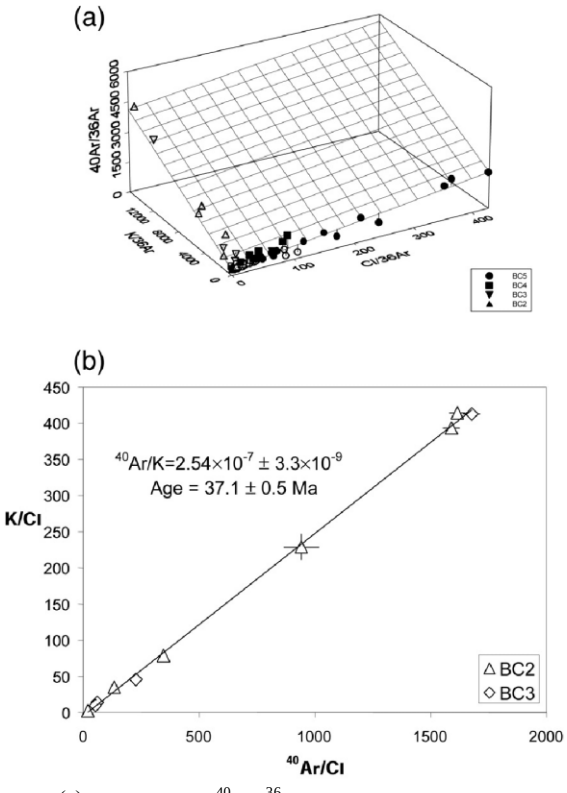

Fig. 7. (a) Multi-isotope, $^{40}Ar–^{36}Ar–K–Cl$, 3D correlation plot for Bingham Canyon, a total of six samples (BC2, BC3 and BC4 and (BC5-A, BC5-B and BC5-C)) have been plotted and are compatible with the age determined. As for Fig. 6, solid symbols represent in vacuo crushing analysis and open symbols represent step heating analysis. Data points obtained by in vacuo crushing analysis are rich in $^{40}Ar_E$ and Cl so lie along the $Cl/^{36}Ar$ axis. (b) $^{40}Ar/Cl$ Vs. K/Cl for stepped heating analysis of K-rich samples BC2 and BC3. The age determined of, 37.1 ± 0.5 Ma is comparable with previously published K–Ar ages in terms of both accuracy and precision.

between K and $^{40}Ar_R$ enabling the $^{40}Ar_R/K$ ratio and hence an age to be determined (Table 7). The age and corresponding error can also be determined through correcting $^{40}Ar/^{36}Ar$ for $^{40}Ar_E$, based on the $^{40}Ar_E/Cl$ ratio determined during in vacuo crushing and plotting the corrected $^{40}Ar/^{36}Ar$ value against $K/^{36}Ar$ on a conventional isochron plot (Turner and Bannon, 1992). For data from Bingham Canyon (samples BC2 and BC3), the effect of the $^{40}Ar_E$ correction is negligible so the age was determined from a conventional three-isotope diagram (Fig. 7b).

6. Significance of the mineralisation ages

The ages of mineralisation at Globe Miami and Pinto Valley porphyry copper deposits derived from the quartz data are 61.7 ± 3.4 and 63.2 ± 8.0 Ma (1σ error), respectively. The relatively large error on the age of Pinto Valley results from it having the lowest $^{40}Ar_R/^{40}Ar_E$ ratio of all the deposits studied and therefore the largest correction for $^{40}Ar_E$. The ages obtained for Globe-Miami and Pinto Valley are indistinguishable, within error from the published K–Ar biotite ages for the mineralisation at both deposits ~ 59 Ma (Creasey, 1980).

The age determined for Ray at 65.3 ± 1.5 is in good agreement with the mean K–Ar age of hydrothermal biotite of 65.4 Ma (Banks et al., 1972). This result is of particular importance as the previous age determinations were ambiguous (Banks et al., 1972). The Granite Mountain Porphyry, known from cross-cutting relationships to be the third of five intrusive phases and to predate the ore body, yielded a range in ages of 3.5 Ma with a mean of 60.8 Ma. This is considerably younger than the 65.4 Ma age of the hydrothermal biotite that cross-cuts the Granite Mountain Porphyry (Banks et al., 1972). The authors were divided on how best to interpret this discrepancy; one possibility was that the age of the hydrothermal biotite was anomalously old due to the presence of $^{40}Ar_E$. The mineralisation must then be younger than 60.8 Ma, the age of the Granite Mountain Porphyry (Banks et al., 1972). An alternative explanation is that $^{40}Ar_R$ loss lowered the apparent age of the Granite Mountain Porphyry. In this model, the K–Ar age of the hydrothermal biotite (65 Ma) represents the age of mineralisation and the five intrusive phases must have been emplaced by this time (Banks et al., 1972). One reason for choosing the second explanation is that Ar loss would logically have occurred during heating events associated with repeated intrusions and hydrothermal alteration. In addition, the amount of $^{40}Ar_E$ trapped in biotite is likely to be small when compared to the amount of $^{40}Ar_R$ produced by such a K-rich mineral in ~ 60 Ma. The Ar–Ar age determined in this study, which has been corrected for $^{40}Ar_E$, supports this view and confirms 65 Ma as the age of mineralisation.

The age of mineralisation at Silverbell derived from the hydrothermal quartz data is 55.8 ± 1.8,

Table 7
Chronology of the porphyry copper deposits studied[a]

Deposit	K–Ar age (Ma)	References	Rock type/mineral dated	Ar–Ar age (Ma)
Bingham Canyon	39.4–36.6	Warnaars et al. (1978)	Hornblende, augite, biotites, from fresh and altered monzonite	37.1 ± 0.5
Silverbell	67	Livingston et al. (1968), Mauger (1966)	Quartz monzonite, biotite	55.8 ± 1.8
	67.1 ± 2	Livingston (1973)		
Globe-Miami	59.5 ± 0.3	Creasey (1980)	Potassically altered porphyry phase of the Shultze granite	61.7 ± 3.4
Pinto Valley	59.1 ± 0.5	Creasey (1980)	Massive secondary biotite from the Lost Gulch quartz monzonite and potassically altered Gold Gulch granodiorite	63.2 ± 8.0
Ray	65.6, 65.2	Banks et al. (1972)	Hydrothermal biotite	65.3 ± 1.5

[a] Previously published K–Ar ages have been included to enable comparison with Ar–Ar ages (1σ error) determined on vein quartz in this study.

which is significantly younger than the K–Ar age of 67 Ma determined for igneous biotite (Mauger, 1966). At present, we do not have a good explanation for this discrepancy, it may be that the biotite analysed by Mauger (1966) formed during an earlier event unrelated to the mineralisation.

The precise age determined for the mineralisation at Bingham Canyon of 37.1 ± 0.5 Ma, is indistinguishable from the K–Ar age of the youngest hydrothermally altered biotites at 36.6 ± 0.3 Ma (Warnaars et al., 1978). They are also in good agreement with laser Ar–Ar ages determined for three different vein samples; 37.7 ± 1.4, 37.4 ± 2.8 and 39.9 ± 2.9 Ma (Irwin and Roedder, 1995). The Bingham stock has an age of 39.8 ± 0.4 so our current data confirms significant hydrothermal activity occurred over a period of approximately 2–3 Ma.

7. Conclusions

Three noble gas extraction techniques have been applied to vein quartz associated with porphyry copper deposits. Some advances have been made in laser ablation, which has been successfully applied to the analysis of small groups of fluid inclusions. The similarity of the average laser ablation Br/Cl value to the bulk value determined by combined in vacuo crushing and stepped heating, indicates that laser ablation releases noble gases from both solid and fluid phases present in fluid inclusions; allowing immediate determination of halogen compositions. In vacuo crushing preferentially samples fluid phases, while step heating of the crushed residue preferentially samples solid phases. The complimentary behaviour of the two bulk extraction techniques has been shown to be advantageous in determination of mineralisation ages by the Ar–Ar technique. Noble gases are unfractionated by daughter minerals; this means noble gas data obtained by in vacuo crushing can be used to investigate fluid origin. However, where daughter minerals exist, it has been found that halogen analyses benefit from the use of stepped heating in conjunction with crushing, enabling 'bulk' values to be calculated. In most cases, Cl determined by in vacuo crushing can be plotted against noble gas isotopes without seriously distorting the data.

The accuracy of age determinations obtained from quartz vein inclusions has been demonstrated by the close agreement of the ages with existing K–Ar studies, especially at Bingham Canyon where the precision of the two techniques are comparable. The value of the quartz inclusion technique has been further demonstrated by its ability to distinguish between two proposed ages for Ray, where the mineralisation age has been confirmed as 65 Ma. This was made possible by correcting K-rich step heating data for $^{40}Ar_E$ based on $^{40}Ar_E/Cl$ ratios determined during crushing analysis. The ages of many ore minerals cannot be determined directly by conven-

tional isotopic methods and especially where mineralisation is not associated with an igneous system the mineralisation age is often only loosely constrained by geological relationships. Consequently, there is a large potential for Ar–Ar age determinations based on quartz in hydrothermal systems. Although the quartz veins analysed in this study are rich in syngenetic mica, the poorest being Pinto Valley which contains $< 0.3\%$, the potential for resolving solid and fluid phases has been clearly demonstrated. A challenge for the future is to apply the methods outlined here to samples with an increasingly low mica content. Provided the fluid inclusions contain sufficient K hosted by the daughter mineral sylvite, it should be possible to resolve $^{40}Ar_E$ in the fluid from $^{40}Ar_R$ in the solid; meaning theoretically an age could be determined from fluid inclusions and daughter minerals alone.

Acknowledgements

We wish to thank D. Blagburn and B. Clementson for technical support in the noble gas laboratory, and C. Thrower for help with sample preparation. J. Ford, S. Titley, C. Phillip, and the ASARCO geologists; R. Cummings, E. John, D. Laux, S. Anzalone, G. Lenzie are thanked for assistance with sample collection. The comments of the reviewers, J.K. Bohlke, F.M. Stuart and S. Kelley, was appreciated. Funding was provided by a NERC studentship (MK) and a Royal Society university research fellowship (RB).

References

Andrews, J.N., Lee, D.J., 1979. Inert gases in groundwater from the Bunter Sandstone of England as indicaters of age and palaeoclimate trends. J. Hydrol. 41, 233.

Banks, N.G., Cornwall, H.R., Silberman, M.L., Creasey, S.C., Marvin, R.F., 1972. Chronology of intrusion and ore deposition at Ray, Arizona: Part I. K–Ar ages. Econ. Geol. 67, 864–878.

Bohlke, J.K., Irwin, J.J., 1992a. Laser microprobe analyses of noble gas isotopes and halogens in fluid inclusions: analyses of microstandards and synthetic inclusions in quartz. Geochim. Cosmochim. Acta 56, 187–201.

Bohlke, J.K., Irwin, J.J., 1992b. Laserprobe analyses of Cl, Br, I, and K in fluid inclusions: implications for the sources of salinity in some ancient hydrothermal fluids. Geochim. Cosmochim. Acta 56, 203–225.

Bohlke, J.K., Irwin, J.J., 1992c. Brine history indicated by argon, krypton, chlorine, bromine, and iodine analyses of fluid inclusions from the Mississippi Valley type lead–fluorite–barite deposits at Hansonburg, New Mexico. Earth Planet. Sci. Lett. 110, 51–66.

Cloke, P.L., Kesler, S.E., 1979. The halite trend in hydrothermal solutions. Econ. Geol. 74, 1823–1831.

Creasey, S.C., 1980. Chronology of intrusion and deposition of porphyry copper ores, Globe-Miami District, Arizona. Econ. Geol. 75, 830–844.

Crocetti, C.A., Holland, H.D., 1989. Sulfur–lead isotope systematics and the composition of fluid inclusions in galena from the Viburnum Trend, Missouri. Econ. Geol. 84, 2196–2216.

Fontes, J.Ch., Matray, J.M., 1993. Geochemistry and origin of formation brines from the Paris Basin, France. Chem. Geol. 109, 149–175.

Holser, W.T., 1979. Trace elements and isotopes in evaporites. In: Burns, R.G. (Ed.), Marine Minerals: Mineralogical Society of America Short Course Notes. Reviews in Mineralogy, pp. 295–346.

Irwin, J.J., Reynolds, J.H., 1995. Multiple stages of fluid trapping in the Stripa granite indicated by laser microprobe analysis of Cl, Br, I, K, U, and nucleogenic plus radiogenic Ar, Kr, and Xe in fluid inclusions. Geochim. Cosmochim. Acta 59 (2), 355–369.

Irwin, J.J., Roedder, E., 1995. Diverse origins of fluid inclusions at Bingham (Utah, USA), Butte (Montana, USA), St. Austell (Cornwall, UK) and Ascension Island (mid-Atlantic, UK), indicated by laser microprobe analysis of Cl, K, Br, I, Ba, Te, U, Ar, Kr, and Xe. Geochim. Cosmochim. Acta 59 (2), 295–312.

Johnson, L., Burgess, R., Turner, G., Milledge, J.H., Harris, J.W., 2000. Noble gas and halogen geochemistry of mantle fluids: comparison of African and Canadian diamonds. Geochim. Cosmochim. Acta 64, 717–732.

Kelley, S., Turner, G., Butterfield, A.W., Shepherd, T.J., 1986. The source and significance of argon isotopes in fluid inclusions from areas of mineralization. Earth Planet. Sci. Lett. 79, 303–318.

Kendrick, M.A., Burgess, R., Pattrick, R.A.D., Turner, G., 2001. Fluid inclusion noble gas (He, Ar, Kr, Xe) and halogen (Cl, Br, I) evidence on the origin of Cu-Porphyry mineralizing fluids. Geochim. et Cosmochim. Acta (in press).

Kennedy, B.M., Lynch, M.A., Reynolds, J.H., Smith, S.P., 1985. Intensive sampling of noble gases in fluids at Yellowstone: I. Early overview of the data, regional patterns. Geochim. Cosmochim. Acta 49, 1251–1261.

Kesler, S.E. et al., 1995. Na–Cl–Br systematics of mineralizing brines in Mississippi Valley-type deposits. Geology 23 (7), 641–644.

Livingston, D.E., 1973. A plate tectonic hypothesis for the genesis of porphyry copper deposits of the southern basin and range province. Earth Planet. Sci. Lett. 20, 171–179.

Livingston, D.E., Mauger, R.L., Damon, P.E., 1968. Geochronol-

ogy of the emplacement enrichment and preservation of Arizona porphyry copper deposits. Econ. Geol. 63, 30–36.

Mauger, R.L., 1966. A petrographic and geochemical study of Silverbell and Pima mining districts, Pima county, Arizona. PhD Thesis, University of Arizona, Tucson.

Mazor, E., 1972. Paleotemperatures and other hydrological parameters deduced from noble gases dissolved in groundwaters; Jordan Rift Valley, Israel. Geochim. Cosmochim. Acta 36, 1321–1336.

Mazor, E., Wasserburg, G.J., 1965. Helium, neon, argon, krypton and xenon in gas emanations from Yellowstone and Lassen Volcanic National Parks. Geochim. Cosmochim. Acta 29, 443–454.

O'Nions, R.K., Ballentine, C.J., 1993. Rare gas studies of basin scale fluid movement. Philos. Trans. R. Soc. London, Ser. A 344, 141–156.

Qui, H.-N., 1996. 40Ar–39Ar dating of the quartz samples from two mineral deposits in western Yunnan (SW China) by crushing in vacuum. Chem. Geol. 127, 211–222.

Rama, S.N.I., Hart, S.R., Roedder, E., 1965. Excess radiogenic argon in fluid inclusions. J. Geophys. Res. 70, 509–511.

Siemann, M.G., Schramm, M., 2000. Thermodynamic modelling of the Br partition between aqueous solutions and halite. Geochim. et Cosmochim. Acta 64, 1681–1693.

Turner, G., 1988. Hydrothermal fluids and argon isotopes in quartz veins and cherts. Geochim. Cosmochim. Acta 52, 1443–1448.

Turner, G., Bannon, M.P., 1992. Argon isotope geochemistry of inclusion fluids from granite-associated mineral veins in southwest and northeast England. Geochim. Cosmochim. Acta 56, 227–243.

Viets, J.G., Hofstra, A.H., Emsbo, P., 1996. Solute compositions of fluid inclusions in sphalerite from North American and European Mississippi Valley-Type ore deposits: ore fluids derived from evaporated seawater. Soc. Econ. Geol., Spec. Publ. 4, 465–482.

Warnaars, F.W., Smith, W.H., Bray, R.E., Lanier, G., Shafiqullah, M., 1978. Geochronology of igneous intrusions and porphyry copper mineralisation at Bingham, Utah. Econ. Geol. 73, 1242–1249.

Zaikowski, A., Kosanke, B.J., Hubbard, N., 1987. Noble gas composition of deep brines from the Palo Duro Basin, Texas. Geochim. Cosmochim. Acta 51, 73–84.